Effect of pH on the stability of passivating gel layers formed on International Simple Glass

M. Fournier, T. Ducasse, A. Perez, A. Barchouchi, D. Daval, S. Gin

Effect of pH on the stability of passivating gel layers formed on International Simple Glass

Maxime Fournier[a], Thomas Ducasse[a], Anne Pérez[b,c], Ayoub Barchouchi[a], Damien Daval[b], Stéphane Gin[a]

[a] CEA, DEN, DE2D, SEVT, F-30207 Bagnols sur Cèze, France

[b] LHyGeS, CNRS, Université de Strasbourg, UMR 7517, 1 rue Blessig 67084 Strasbourg, France

[c] LGE, Université Paris-Est, Laboratoire Géomatériaux et Environnement, (EA 4508), UPEM, 77454 Marne-la-Vallée, France

Corresponding author: Maxime Fournier
Postal address: CEA Centre de Marcoule
DEN/DE2D/SEVT/LCLT, Bat. 208
BP 17171
30207 Bagnols sur Cèze Cedex
France
Tel.: +33 466797710
E-mail address: maxime.fournier@cea.fr

Abstract (≤ 300 words)

It is known for decades that silica saturated solutions allow borosilicate glass to dissolve much slower than in deionized water. The present study assesses this assertion in the specific case of the International Simple Glass, a 6-oxide borosilicate glass of nuclear interest, which we altered between pH = 1 and 10.7 at 90 °C. Depending on the stage of reaction, aqueous silica can promote either the formation of a passivating gel layer on the glass surface or the precipitation of certain secondary phases at the expense of the passivating gel. We demonstrate a negligible effect of aqueous silica at acidic pH and a marked effect beyond $pH_{90\,°C}$ = 7, ensuring a better glass chemical durability. At higher reaction progress and above $pH_{90\,°C}$ = 9.5, this effect becomes negative due to the formation of secondary phases such as hydroxides or zeolites.

Keywords

ISG, nuclear glass, amorphous silica, pH.

Graphical abstract (readable at a size of 5 × 13 cm using a resolution of 96 dpi)

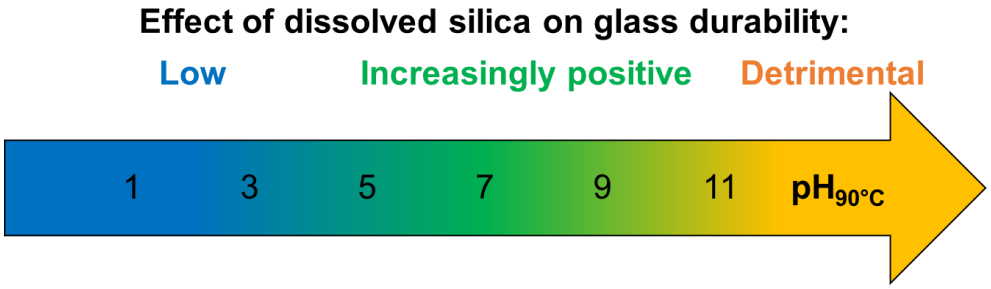

Highlights (3 to 5 bullet points, ≤ 85 characters)

- No effect of SiO_2(aq) on the dissolution rate at acidic pH
- Aqueous SiO_2 slows glass dissolution at $pH_{90\,°C} \geq 7$ and low reaction progress
- Aqueous SiO_2 fasters glass dissolution at $pH_{90\,°C} \geq 9.5$ and low reaction progress

1. Introduction

Some countries like France, Japan, Russia, India or Great Britain have chosen to reprocess their spent nuclear fuel. The minor actinides and fission products arising from this reprocessing are vitrified in borosilicate or, to a lesser extent, phosphate glasses. In France, the vitrified waste form, usually called “nuclear glass”, will be packed in carbon steel containers and eventually stored in a deep claystone formation, stable and with low permeability. The safety assessment of the geological repository relies on the performance of the different barriers and thus partly on the chemical durability and radiation resistance of the glass. Although research on nuclear glass durability began a few decades ago, it is still an intense investigation field [1].

In contact with groundwater, glass dissolves and transforms into more stable phases at a rate highly dependent on geochemical conditions. The formation of a Si-rich passivating layer (also called “gel”) allows, under the most favorable conditions, to guarantee a glass package lifetime of several hundred thousand years [2]. For the same glass, the composition and the structure of the gel vary according to the environmental parameters, in particular the pH and the composition of the solution. The formation of the gel competes with the formation of other secondary minerals [3-9]. As an illustration, some experiments show the presence of gel dissolution patterns under neoformed secondary phases [10, 11]. Finally, the geochemical modeling of nuclear glasses alteration is based on the respective solubilities of the gel and secondary phases [12, 13].

The presence of aqueous silica [14-19] has two major effects on the glass: on the one hand, it decreases the affinity of the matrix dissolution reaction ($SiO_2 + 2\ H_2O \rightarrow H_4SiO_4$) and on the other hand, it favors the backward reaction of silica condensation. This reaction accounts for the formation of the gel layer which can, in some circumstances, be transport-limiting. Aqueous silica is not the only dissolved species which can affect glass durability. Actually, most dissolved species can play a direct role either on the reaction of hydrolysis of the –Si–

O–Si– bonds [20, 21] or indirectly, through the pH or the gel formation [6, 22-24]. Because the pH of leaching solutions is generally buffered around 9–9.5 by boron released by the glass ($B(OH)_3 + H_2O \rightarrow B(OH)_4^- + H^+$, $pK_a = 9.14$ at room temperature), and since the pH of many natural groundwaters ranges between 6 and 8, many studies were conducted between pH = 7 and 9.5. However, some disposal designs would lead to more alkaline pH conditions [25] raising the question of the gel stability beyond the threshold of 9.5. Besides, below pH 7, the role of aqueous silica is unclear.

This study thus reports on the behavior of the dissolution of an international reference glass ISG (International Simple Glass) [26], a 6-oxide borosilicate glass, in solutions saturated or not with respect to amorphous silica at 90 °C for $pH_{90\,°C}$ ranging between 1 and 10.7. Beyond this latter pH, it becomes experimentally challenging to saturate the solution. Two ratios between the reactive surface area developed by the glass powder and the volume of solution are used. These two ratios are distant from two orders of magnitude and they are complementary over the entire pH range of the study while allowing (i) to maximize the difference of silica concentrations between a pre-saturated solution and a solution where silica comes solely from the glass dissolution glass and (ii) to measure the boron concentration with sufficient analytical precision.

2. Material and Methods

2.1. Preparation of the material

The tests were conducted using the ISG, which composition is given in Table 1. ISG ingots were prepared by MO-SCI Corporation (Rolla, MO, USA) [27] and provided by Savannah River National Laboratory (Aiken, SC, USA). Two glass powders were prepared from successive steps of crushing with a vario-planetary mill and sieving to obtain the 125-250 µm and 20-40 µm size fractions. Powders were washed by an iterative decantation process to remove fine particles using acetone and absolute ethanol according to Stokes' law.

ISG	SiO_2	B_2O_3	Na_2O	Al_2O_3	CaO	ZrO_2
Oxide wt%	56.2 ± 1.5	17.3 ± 0.9	12.2 ± 0.7	6.1 ± 0.8	5.0 ± 0.6	3.3 ± 0.5

Table 1: ISG composition expressed in oxide weight percent.

2.2. Leaching tests

Static leaching tests were performed at 90 ± 2 °C in perfluoroalkoxy vessel. Two test series were conducted: the first (S1) with a glass-surface-area-to-solution-volume (*S*/*V*) ratio of 60 m^{-1} using the 125-250 µm size fraction, and the second (S2) with *S*/*V* = 10 000 m^{-1} using the 20-40 µm size fraction. The reactive surfaces correspond to the geometric surfaces—assimilating glass grains to spheres—corrected by a 1.3-factor to take into account the non-sphericity of the glass grains [28].

Leaching tests (Table 2) were conducted in solutions saturated with respect to amorphous silica ("Sat" test series) at various pH, or in solutions with the same pH and initially devoid of aqueous silica ("Blk" test series). The acid solutions were prepared by diluting nitric acid (65%, Merck Suprapur®) in 18 MΩ·cm ultrapure water, and the basic solutions by dissolving KOH pellets (Merck Emsure®). The amounts of silica introduced to reach saturation at 90 °C in "Sat" test series were calculated using the Chess code [29]. For $pH_{90\,°C} \geq 9.5$, silica-containing solutions were prepared by dissolving amorphous silica for about a week at 90 °C under stirring. For lower pH, the solution prepared with a $pH_{90\,°C}$ of 9.5 was split and acidified. The silica concentration of each solution was checked using a UV-visible spectrometer (Cary® 50 Scan UV-Vis) according to a method analogous to ASTM D859-10 [30]. During the tests, the pH was manually controlled at the set point by regular additions of micro volumes of concentrated solutions of HNO_3 or KOH.

Test name	Test series	*S/V* (m^{-1})	*T* (°C)	$pH_{90°C}$	C_{Si} ($mg \cdot L^{-1}$)	Duration (d)
S1-Sat-1	1	60	90	1	$3.1 \cdot 10^2$	365
S1-Blk-3	1	60	90	3	0	365
S1-Sat-3	1	60	90	3	$3.0 \cdot 10^2$	365
S1-Blk-7	1	60	90	7	0	365
S1-Sat-7	1	60	90	7	$1.5 \cdot 10^2$	365
S1-Sat-8	1	60	90	8	$1.8 \cdot 10^2$	365
S1-Sat-9	1	60	90	9	$2.8 \cdot 10^2$	365
S1-Blk-9.5	1	60	90	9.5	0	365
S1-Sat-9.5	1	60	90	9.5	$7.4 \cdot 10^2$	365
S1-Sat-9.8	1	60	90	9.8	$1.4 \cdot 10^3$	365
S1-Blk-10.1	1	60	90	10.1	0	365
S1-Sat-10.1	1	60	90	10.1	$3.9 \cdot 10^3$	365
S1-Sat-10.3	1	60	90	10.3	$1.2 \cdot 10^4$	365
S2-Blk-9.5	2	10 000	90	9.5	0	379
S2-Sat-9.5	2	10 000	90	9.5	$7.4 \cdot 10^2$	379
S2-Blk-9.8	2	10 000	90	9.8	0	379
S2-Blk-9.8	2	10 000	90	9.8	$1.4 \cdot 10^3$	379
S2-Blk-10.1	2	10 000	90	10.1	0	379
S2-Sat-10.1	2	10 000	90	10.1	$3.9 \cdot 10^3$	379
S2-Blk-10.3	2	10 000	90	10.3	0	379
S2-Sat-10.3	2	10 000	90	10.3	$1.2 \cdot 10^4$	379
S2-Blk-10.7	2	10 000	90	10.7	0	379
S2-Sat-10.7	2	10 000	90	10.7	$2.7 \cdot 10^4$	379

Table 2: Characteristics of Series 1 and 2 tests, including glass-surface-area-to-solution-volume (*S*/*V*) ratio, temperature (*T*), pH to be maintained measured at 90 °C, initial silicon concentration (C_{Si}), and total duration.

2.3. Solution analyses

0.5 mL solution samples were taken at 1, 3, 7, 14, 28 days, 3 months and 1 year. Samples were ultrafiltered at 10 000 D, acidified with 0.5 N HNO_3 and analyzed by Inductively coupled plasma atomic emission spectroscopy (ICP-OES, Thermo Scientific iCAP™ 6000 Series) for boron and silicon concentrations. As boron is known to be a glass alteration tracer, its concentration was used for the calculation of the altered glass percentage, %AG, from a mass balance taking into account the volume variation (Equation 1).

$$\%\mathrm{AG} = \frac{C_i(t) \times V(t) + \sum_{j=1}^{t-1} C_i(j) \times V_S(j)}{m \times x_i} \quad (1)$$

with $C_i(t)$ the mass concentration of element *i* at time *t*, x_i the mass fraction of element *i* in the glass composition, $V(t)$ the solution volume at time *t*, $V_S(j)$ the volume of the *j*-th sampling, and *m* the mass of glass.

The equivalent thickness of altered glass, eTh(B), was calculated as a function of time using Equation 2, where r_0 is the glass particles radius at $t = 0$ and r_t its radius at a time *t*.

$$\mathrm{eTh(B)} = r_0 - r_t = r_0 \times \left[1 - (1 - \%\mathrm{AG})^{\frac{1}{3}}\right] \quad (2)$$

2.4. Solid analyses

X-ray diffraction (XRD). XRD patterns were acquired with a Phillips X'PERT Pro diffractometer equipped with a Cu-Kα monochromatic source (λ = 1.5418 Å) operating at 40 mA, 40 kV in Bragg-Brentano geometry. Scans were taken for 2θ ranges ranges from 4° to 80° with a speed of 0.11°·min^{-1} and a step of 0.017° (2θ) using amorphous silica sample holders. The XRD patterns were processed using the DIFFRAC.EVA v. 4.2 (Bruker) software and compared to the reference patterns of the International Center for Diffraction Data PDF-4+ 2018 RDB.

Scanning electron microscopy (SEM). The solid samples taken at the end of the leaching experiments were rinsed, dried, coated with a carbon deposit, and observed with a Zeiss Merlin scanning electron microscope operated with an accelerating voltage of 15 kV and coupled with a lithium doped silicon detector for energy dispersive X-ray spectrometry.

3. Results

3.1. S1 test series: low *S*/*V* ratio

In S1 test series, the pH values were generally maintained at the set values within ± 0.3 pH unit, with the exception of a few excursions, especially in the first 10 days of the $pH_{90\,°C}$ = 7

tests, where the pH control was the most difficult (Figure A.1). The evolutions of silicon concentrations are given in Table 3.

In the “S1-Blk” tests (Figure 1.a), the most important altered glass thicknesses are reached at $pH_{90°C}$ = 3 and the least important at $pH_{90°C}$ = 9.5. Between $pH_{90°C}$ = 3 and $pH_{90°C}$ = 9.5, the altered thicknesses gradually decrease; above $pH_{90\ °C\ =}$ 9.5, the altered glass thicknesses increase with a sharp variation in the alteration rate between 28 and 91 days, associated with the precipitation of calcium silicate hydrate-like phases (CSH) [27, 31] evidenced by SEM (Figure 2.a) but that cannot be identified by XRD because of the absence of diffraction peaks.

In the “S1-Sat” tests (Figure 1.b), the same evolution of the altered glass thicknesses as a function of pH as in the “S1-Blk” tests is observed: a decrease between $pH_{90°C}$ = 3 and $pH_{90°C}$ = 9.5 and an increase beyond that point. However, it should be noted that eTh(B) at $pH_{90°C}$ = 3 is slightly higher than at $pH_{90°C}$ = 1. From $pH_{90°C}$ = 9.5, only the boron concentration of the last sample at 1 year could be measured because of the high dilution to be made due to the high silica content of these solutions. This result motivated a second test series conducted at higher *S*/*V* ratio (section 3.2). Finally, only small amounts of phyllosilicate-like secondary phases [32, 33] are observed by SEM in these tests (Figure 2.b).

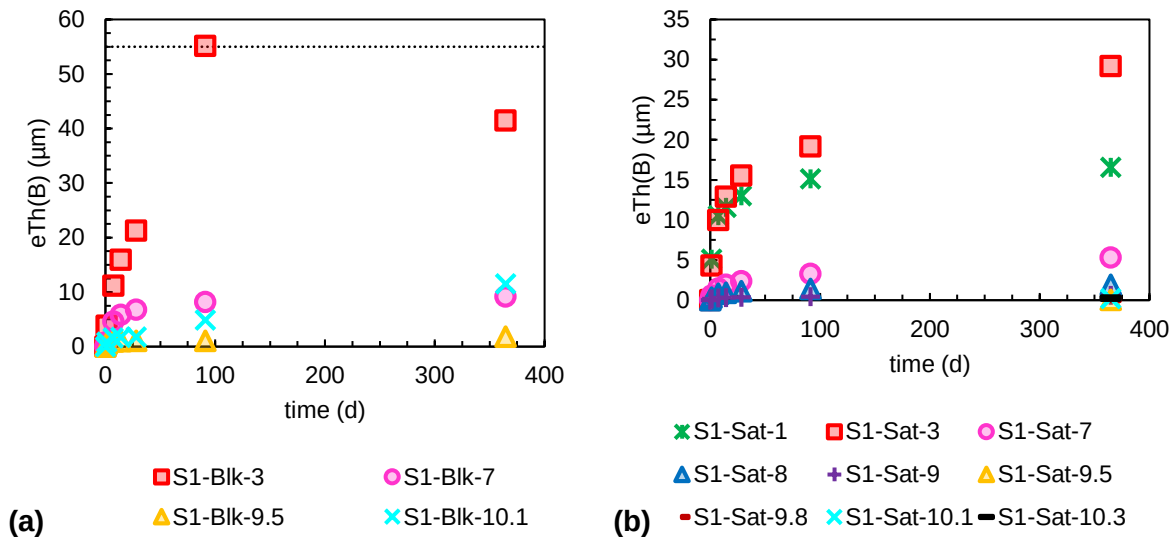

Figure 1: Evolution of the equivalent thicknesses of altered glass calculated from boron concentrations, eTh(B), for the **(a)** S1-Blk and **(b)** S1-Sat test series conducted with an *S*/*V* ratio of 60 m^{-1}. Dotted line represents the total alteration of the glass (%AG = 100). Zoomed-in subfigures are given in Appendix B.

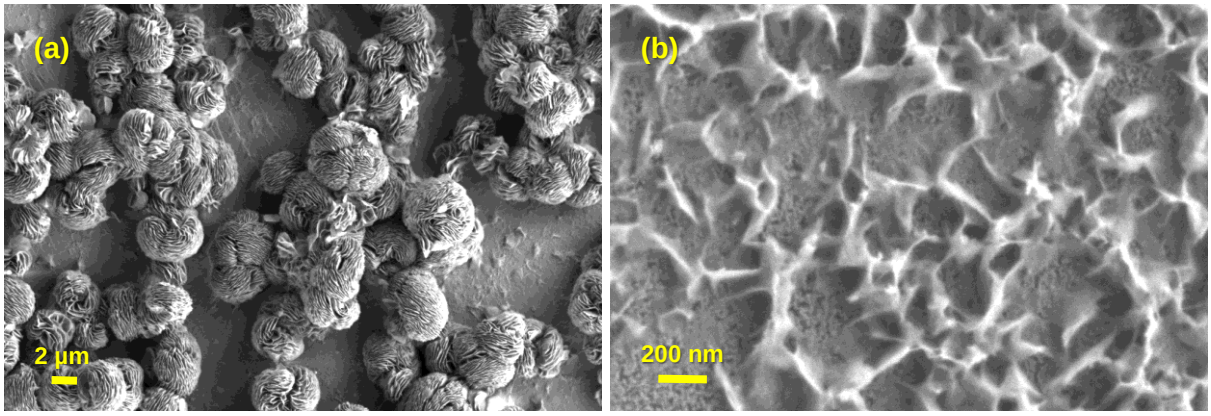

Figure 2: Secondary electrons scanning electron microscope images after 1 year in tests **(a)** S1-Blk-10.1 and **(b)** S1-Sat-10.1.

Time (d)	S1-Sat-1	S1-Blk-3	S1-Sat-3	S1-Blk-7	S1-Sat-7	S1-Sat-8	S1-Sat-9	S1-Blk-9.5	S1-Sat-9.5	S1-Sat-9.8	S1-Blk-10.1	S1-Sat-10.1	S1-Sat-10.3
0	$3.1 \cdot 10^{2}$	3.3	$3.0 \cdot 10^{2}$	2.2	$1.5 \cdot 10^{2}$	$1.8 \cdot 10^{2}$	$2.8 \cdot 10^{2}$	5.7	$7.4 \cdot 10^{2}$	$1.3 \cdot 10^{3}$	$2.4 \cdot 10^{1}$	$3.8 \cdot 10^{3}$	$1.2 \cdot 10^{4}$
1.2	$2.9 \cdot 10^{2}$	$8.4 \cdot 10^{1}$	$3.1 \cdot 10^{2}$	$1.7 \cdot 10^{1}$	$1.5 \cdot 10^{2}$	$1.5 \cdot 10^{2}$	$2.5 \cdot 10^{2}$	$2.0 \cdot 10^{1}$	$6.4 \cdot 10^{2}$	$1.2 \cdot 10^{3}$	$3.6 \cdot 10^{1}$	$3.4 \cdot 10^{3}$	$9.9 \cdot 10^{3}$
7.2	$3.1 \cdot 10^{2}$	$3.3 \cdot 10^{1}$	$3.2 \cdot 10^{2}$	$5.9 \cdot 10^{1}$	$1.4 \cdot 10^{2}$	$1.5 \cdot 10^{2}$	$2.8 \cdot 10^{2}$	$3.6 \cdot 10^{1}$	$6.3 \cdot 10^{2}$	$1.2 \cdot 10^{3}$	$6.7 \cdot 10^{1}$	$3.5 \cdot 10^{3}$	$1.1 \cdot 10^{4}$
14.2	$3.4 \cdot 10^{2}$	$4.6 \cdot 10^{1}$	$3.1 \cdot 10^{2}$	$6.3 \cdot 10^{1}$	$1.4 \cdot 10^{2}$	$1.5 \cdot 10^{2}$	$2.5 \cdot 10^{2}$	$4.2 \cdot 10^{1}$	$5.9 \cdot 10^{2}$	$1.2 \cdot 10^{3}$	$6.7 \cdot 10^{1}$	$3.4 \cdot 10^{3}$	$9.7 \cdot 10^{3}$
28.2	$4.9 \cdot 10^{2}$	$5.5 \cdot 10^{1}$	$3.2 \cdot 10^{2}$	$6.6 \cdot 10^{1}$	$1.4 \cdot 10^{2}$	$1.5 \cdot 10^{2}$	$2.5 \cdot 10^{2}$	$4.4 \cdot 10^{1}$	$5.5 \cdot 10^{2}$	$1.0 \cdot 10^{3}$	$7.5 \cdot 10^{1}$	$2.8 \cdot 10^{3}$	$1.0 \cdot 10^{4}$
91.1	$5.9 \cdot 10^{2}$	$9.3 \cdot 10^{1}$	$3.6 \cdot 10^{2}$	$7.6 \cdot 10^{1}$	$1.8 \cdot 10^{2}$	$1.6 \cdot 10^{2}$	$2.8 \cdot 10^{2}$	$6.2 \cdot 10^{1}$	NA	$1.6 \cdot 10^{3}$	$1.4 \cdot 10^{2}$	NA	$1.8 \cdot 10^{4}$
364.6	$5.6 \cdot 10^{2}$	$6.0 \cdot 10^{2}$	$9.5 \cdot 10^{2}$	$2.5 \cdot 10^{2}$	$3.3 \cdot 10^{2}$	$2.6 \cdot 10^{2}$	$4.7 \cdot 10^{2}$	$1.4 \cdot 10^{2}$	$8.4 \cdot 10^{2}$	$1.3 \cdot 10^{3}$	$5.1 \cdot 10^{2}$	$4.0 \cdot 10^{3}$	$1.2 \cdot 10^{4}$

Table 3: Silicon concentrations expressed in $g \cdot m^{-3}$ for S1 test series (NA: not analyzed).

Time (d)	S2-Blk-9.5	S2-Sat-9.5	S2-Blk-9.8	S2-Sat-9.8	S2-Blk-10.1	S2-Sat-10.1	S2-Blk-10.3	S2-Sat-10.3	S2-Blk-10.7	S2-Sat-10.7
0.0	4.3	$7.2 \cdot 10^{2}$	2.8	$1.8 \cdot 10^{3}$	2.1	$3.8 \cdot 10^{3}$	3.0	$1.1 \cdot 10^{4}$	6.8	$3.5 \cdot 10^{4}$
1.1	$1.9 \cdot 10^{1}$	$6.3 \cdot 10^{2}$	$1.0 \cdot 10^{2}$	$1.2 \cdot 10^{3}$	$1.5 \cdot 10^{2}$	$3.5 \cdot 10^{3}$	$1.1 \cdot 10^{2}$	$1.0 \cdot 10^{4}$	$1.8 \cdot 10^{2}$	$2.7 \cdot 10^{4}$
3.0	$2.1 \cdot 10^{1}$	$6.0 \cdot 10^{2}$	$1.2 \cdot 10^{2}$	$1.1 \cdot 10^{3}$	$1.6 \cdot 10^{2}$	$3.4 \cdot 10^{3}$	$1.2 \cdot 10^{2}$	$9.4 \cdot 10^{3}$	$2.0 \cdot 10^{2}$	$2.9 \cdot 10^{4}$
7.0	$1.9 \cdot 10^{1}$	$6.2 \cdot 10^{2}$	$1.5 \cdot 10^{2}$	$1.2 \cdot 10^{3}$	$1.6 \cdot 10^{2}$	$3.6 \cdot 10^{3}$	$1.3 \cdot 10^{2}$	$9.4 \cdot 10^{3}$	$2.3 \cdot 10^{2}$	$2.5 \cdot 10^{4}$
14.0	$1.9 \cdot 10^{1}$	$5.5 \cdot 10^{2}$	$1.9 \cdot 10^{2}$	$1.3 \cdot 10^{3}$	$1.5 \cdot 10^{2}$	$3.3 \cdot 10^{3}$	$1.2 \cdot 10^{2}$	$1.0 \cdot 10^{4}$	$1.9 \cdot 10^{2}$	$2.5 \cdot 10^{4}$
28.1	$1.9 \cdot 10^{1}$	$3.3 \cdot 10^{2}$	$1.4 \cdot 10^{2}$	$1.1 \cdot 10^{3}$	$1.4 \cdot 10^{2}$	$3.5 \cdot 10^{2}$	$1.7 \cdot 10^{2}$	$8.6 \cdot 10^{3}$	$2.2 \cdot 10^{2}$	$2.5 \cdot 10^{4}$
91.1	$1.2 \cdot 10^{1}$	$5.1 \cdot 10^{2}$	$1.9 \cdot 10^{2}$	$9.4 \cdot 10^{2}$	$1.9 \cdot 10^{2}$	$3.0 \cdot 10^{3}$	$2.0 \cdot 10^{2}$	$8.0 \cdot 10^{3}$	$2.2 \cdot 10^{2}$	$2.4 \cdot 10^{4}$
379.0	$3.6 \cdot 10^{1}$	$5.5 \cdot 10^{2}$	$2.2 \cdot 10^{2}$	$9.5 \cdot 10^{2}$	$3.2 \cdot 10^{2}$	$2.1 \cdot 10^{3}$	$3.5 \cdot 10^{2}$	$1.1 \cdot 10^{4}$	$5.2 \cdot 10^{2}$	$2.5 \cdot 10^{4}$

170 **Table 4:** Silicon concentrations expressed in $g \cdot m^{-3}$ for S2 test series.

3.2. S2 test series: high *S*/*V* ratio

As in the S1 test series, the pH were maintained around the setpoint values during the first 100 days (Figure A.2). However, the pH decreased significantly between 100 days and 1 year without being compensated by alkaline additions. The evolutions of silicon concentrations are given in Table 4. In the “S2-Blk” tests (Figure 3.a, Figure 4.a, Figure 5.a), the equivalent altered thicknesses are close during the first 100 days, increasing slightly with the decrease in pH between 10.7 and 9.5. Between 100 days and a year, only the highest pH ($pH_{90\,°C}$ = 10.7) deviates from this trend by altering more rapidly. The higher altered equivalent thicknesses in this test correlate with the precipitation of secondary phases identified as calcium alumina silicate hydrates by XRD.

In the “S2-Sat” test series (Figure 3.b, Figure 4.b, Figure 5.b), larger amounts of secondary phases are identified: oxyhydroxides, silicates, carbonates and zeolites. The more alkaline is the medium, the larger are the amounts of precipitated crystalline phases after 1 year of leaching, and the higher are the equivalent thicknesses of altered glass. In detail (Figure 5):

- no diffraction peak is observed at $pH_{90\,°C}$ <10.1;
- at $pH_{90\,°C}$ = 10.1: potassium calcium silicon oxide hydrate (PDF 04-012-5493) and potassium sodium silicon oxide (04-014-8491);
- at $pH_{90\,°C}$ = 10.3: potassium calcium silicon oxide hydrate (04-012-5493), potassium hydrogen carbonate (04-013-5503), sodium silicate (00-018-1241), and leucite (00-038-1423);
- at $pH_{90\,°C}$ = 10.7: potassium calcium silicon oxide hydrate (04-012-5493), hydrogen potassium sodium carbonate hydrate (04-010-8201), shlykovite (00-061-0758), phillipsite K (00-034-0542), and leucite (00-038-1423). In addition, the XRD pattern shows a broad reflection around 30° (2θ) which is characteristic of CSH [34, 35].

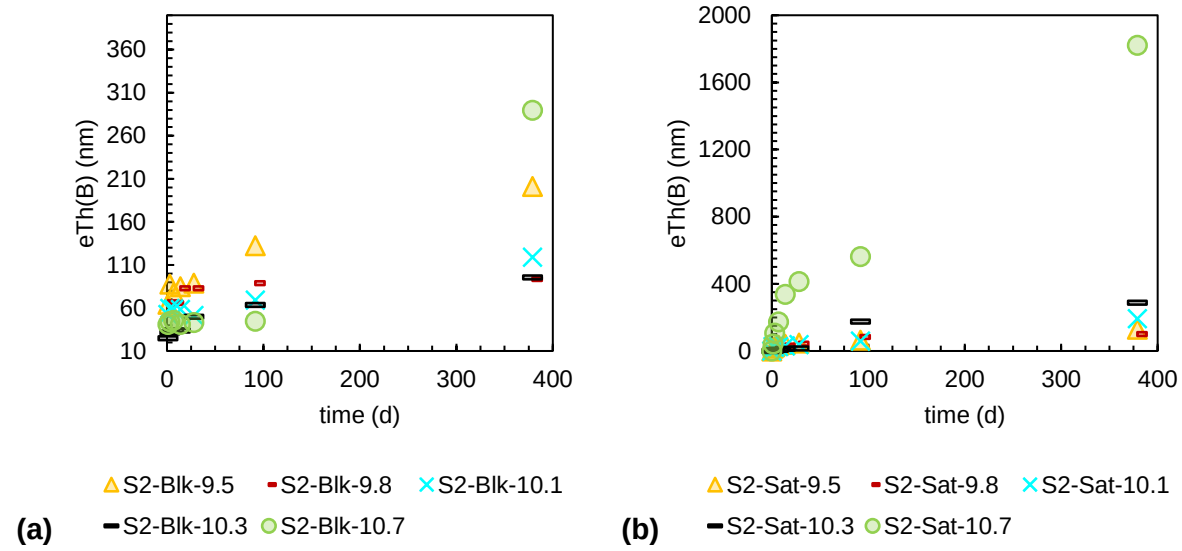

Figure 3: Evolution of the equivalent thicknesses of altered glass calculated from boron concentrations, eTh(B), for the **(a)** S2-Blk and **(b)** S2-Sat test series conducted with an *S*/*V* ratio of 10 000 m^{-1}. Zoomed-in subfigures are given in Appendix B.

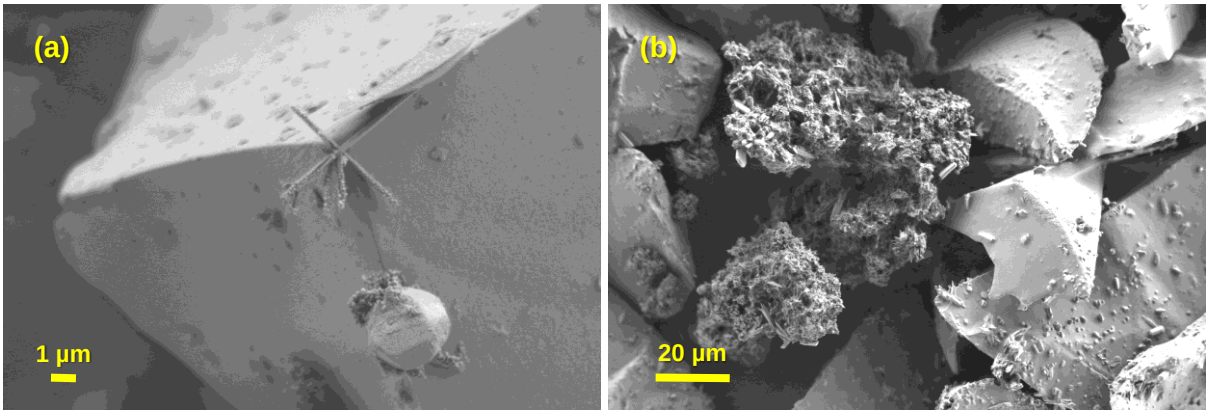

Figure 4: Secondary electrons scanning electron microscope images after 1 year in tests **(a)** S2-Blk-10.3 and **(b)** S2-Sat-10.3.

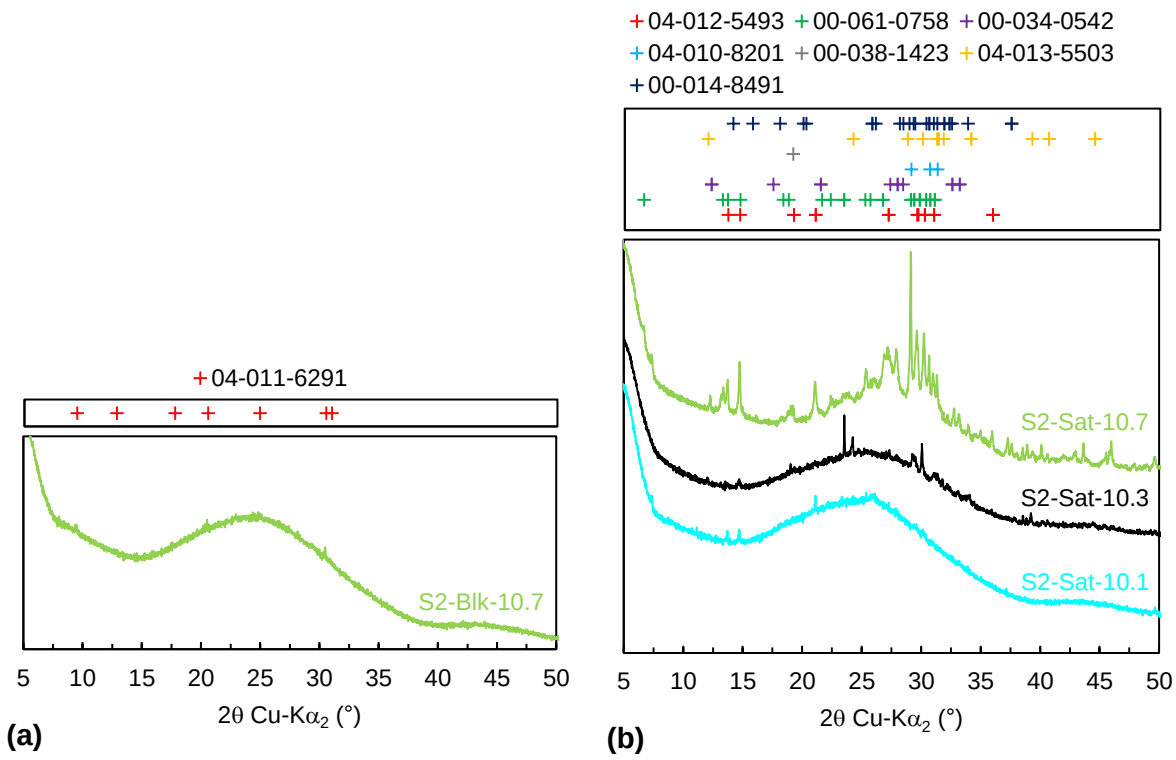

Figure 5: X-ray diffraction patterns of S2 **(a)** "Sat" and **(b)** "Blk" test series. The positions of the major peaks ($I \geq 0.3 \times I_{max}$) of the reference diffractograms (PDF-4+ 2018 RDB, database 4.1801) corresponding to the identified phases are represented: K-Ca-Si oxyhydroxide (PDF 04-012-5493), shlykovite (PDF 00-061-0758), phillipsite-K (PDF 00-034-0542), Na-K carbonate (PDF 04-010-8201), leucite (PDF 00-038-1423), K carbonate (PDF 04-013-5503), K-Na-Si oxide (PDF 04-014-8491), and Ca-Al-Si hydrate (PDF 04-011-6291).

4. Discussion

The choice of a "low" *S*/*V* ratio for S1 test series was made to maintain as long as possible a large difference in silica concentration between the "S1-Sat" test series (aqueous silica-containing solutions) and the "S1-Blk" test series (solutions without silica). However, the results show that this experimental design did not allow for the quantification of the glass alteration in strongly alkaline solutions because of the dilution of the samples—imposed by the high silica concentrations—and required for ICP-OES analysis (e.g. dilution factor > 200 at $pH_{90\,°C}$ = 10.3). To circumvent this shortcoming, S2 test series was conducted with a higher *S*/*V* ratio and focused on alkaline pH. It is, however, more difficult to highlight the effect of the initial saturation of the solution with respect to amorphous silica in such conditions because the solution quickly reach saturation due to the greater surface area of glass. As an example, at $pH_{90\,°C}$ = 9.8, it is theoretically necessary to dissolve 35 µm of glass to reach saturation with respect to amorphous

220 silica at S/V = 60 cm^{-1} against 0.2 µm at S/V = 10 000 cm^{-1}. Both S1 and S2 test series will be discussed in the following.

In the S1 test series and at $pH_{90\,°C}$ = 1, an initial dissolution rate of 3.2 $g \cdot m^{-2} \cdot d^{-1}$ is calculated between 0 and 7 days by linear regression (despite the beginning of inflection of the alteration rate). This value can be compared to that extrapolated from data acquired at 90°C by Inagaki*, et al.* [36] of ≈ 2.5 $g \cdot m^{-2} \cdot d^{-1}$. The fact that these two values are very close, added to the comparison of the "S1-Blk" and "S1-Sat" tests at the pH where both tests were carried out jointly (Figure 6.a and Figure C.1) shows that the effect of aqueous silica on the glass dissolution is negligible at $pH_{90\,°C} \leq 3$. It becomes more significant at $pH_{90\,°C}$ = 7: the equivalent thickness of altered glass is 1.5 to 3 times greater when the reaction is conducted in a Si-rich solution (Figure C.1.b). This difference increases very significantly with the pH, from a factor of ≈ 35 at $pH_{90\,°C}$ = 9.5 to a factor ≈ 60 at $pH_{90\,°C}$ = 10.1. For the two most alkaline pH tested in the S1 test series, the gap due to the initial presence of aqueous silica should probably be even greater before 1 year because the silicon concentrations in the "S1-Blk" test series at 1 year are high ($1.4 \cdot 10^2$ $mg \cdot L^{-1}$ at $pH_{90\,°C}$ = 9.5 and $5.1 \cdot 10^2$ $mg \cdot L^{-1}$ at $pH_{90\,°C}$ = 10.1, Table 3). Therefore, it appears from these tests that aqueous silica acts positively on glass durability from the $pH_{90\,°C} \approx 7$ threshold and this effect increases with pH, at least up to $pH_{90\,°C} \approx 10.1$ for this first test series with a low S/V ratio. This beneficial effect can be interpreted by the quick formation of a passivating layer in the silica-rich solutions [37], while it requires a partial dissolution of the glass in the "Blk" tests to reach saturation.

Unexpectedly, aqueous silica seems to have no direct nor indirect effect on glass alteration in acidic pH. This could be due to several reasons: (i) the rate was calculated from B release; it can be hypothesized that B is preferentially leached out in acidic pH along with alkalis, whose release from the glass is known to be driven by ion-exchange [38-41], (ii) a passivating gel cannot form because condensation reactions are slower in acidic pH than in basic pH [42].

On the one hand, the first hypothesis is supported by the observation that B and Na are released congruently, following a square root-dependent time law until total alteration of the glass (Figure 7.a). Thus, it is plausible that ion-exchange is responsible for the release of Na and that the penetration of hydronium ions into the glass also drives the hydrolysis of B. At $pH_{90\,°C}$ = 3, Si dissolves approximately 20 times slower than B and Na. The preferential release of B and Na with respect to Si suggests the remaining of a thick Si-rich surface layer. This layer may undergo local reorganization limiting the effect of ion exchange and explaining the square root-dependence between time and B and Na releases .The observed preferential leaching of B and Na with respect to Si in acidic conditions also explains why the initial Si concentration in solution is not a determinant parameter in acidic systems. By contrast, at $pH_{90\,°C}$ = 10.1, the three elements dissolve almost at the same rate (Figure 7.a). These results suggest that the processes controlling elemental releases into the solution are less coupled in acidic conditions than in the $pH_{90\,°C}$ range of 7–9.5 where the release of weakly bonded elements such as Na and B is strongly affected by hydrolysis-condensation within the silicate network.

On the other hand, the second hypothesis is similar to the one suggested by Daval*, et al.* [43] to account for the passivating ability of Si-rich layers developed on slow-dissolving wollastonite cleavage planes as opposed to fast-dissolving cleavage planes. More generally, the non-passivating behavior of silica layers developed in acidic solutions has been previously evidenced by the mineralogical community for a series of Fe-free silicate minerals altered in acidic pH solutions, including wollastonite [44], feldspars [45-47] and forsterite [48]. In particular, Wild*, et al.* [47] demonstrated that Si-rich layers formed on labradorite switched from non-passivating at pH ≤ 2.5 to passivating at pH > 2.5, indicating that the threshold pH value for passivation is lower for feldspars than for ISG, indicating that there might be a strong coupling between the intrinsic dissolution rate of the parent phase (which increases with decreasing pH, in the acidic pH range) and the rate of the silica layer condensation/polymerization (which decreases with decreasing pH, in the acidic pH range).

The S2 test series, with the higher *S*/*V* ratio, sheds a different light compared to those of the first series. Indeed, at $pH_{90\,°C}$ = 9.8 and *S*/*V* = 10 000 m^{-1}—pH for which it had been shown that the presence of aqueous silica had a positive effect on the glass durability—, the altered glass fraction is the same, irrespective to the initial aqueous silica concentration of the solution after a year (Figure 6.b and Figure C2). This trend is different at $pH_{90\,°C}$ = 10.1, 10.3, and 10.7, where the glass is significantly more altered in silica-rich solutions. Therefore, the passivating layer, whose formation is favored by the initial presence of aqueous silica, is rapidly destabilized. This destabilization could be linked to the precipitation of Si-rich secondary phases: C(A)SH and zeolites—already known to be at the origin of the so-called “resumption of alteration” phenomenon leading to an acceleration of the glass alteration rate [7, 49]—, carbonates, and also poorly crystallized oxy-hydroxides of silicon, alkaline and alkaline earth which can be sources of elements for the precipitation of zeolites.

For the 3 most alkaline pH of this second test series, a significant difference between the silica concentrations reached in the “Blk” tests (≈ 300 to 500 $g \cdot m^{-3}$) and those in the pre-saturated solutions ($2 \cdot 10^3$ to $2.5 \cdot 10^4$ $g \cdot m^{-3}$) is observed (Figure 6). This difference increases with pH. At $pH_{90°C}$ = 9.5, the difference is small and it is expected that it would be even smaller at longer times, as it was demonstrated according to a 14 year-long experiment that the solution at this pH eventually achieve the equilibrium with amorphous silica [50]. This was made possible because no secondary phases precipitated at this pH. Here, because silicate minerals precipitate above $pH_{90°C}$ = 9.5, they partly control the solution composition. Studies conducted at high pH have shown that precipitation of silicate minerals such as CSH and zeolites is not instantaneous and that there is an induction period during which glass dissolves slowly before alteration resumes [7, 49, 51]. During this so-called “plateau regime”, the solution composition is controlled by various amorphous materials whose composition, structure and properties are poorly known [13, 52, 53]. Then, the mechanisms of formation of these materials are pH-dependent, although the average composition of the alteration layer—deduced from elemental concentrations in solution—varies little: $SiAl_{0.2\pm0.1}Ca_{0.1\pm0.1}Zr_{0.05\pm0.03}$, without showing any trend with pH variations.

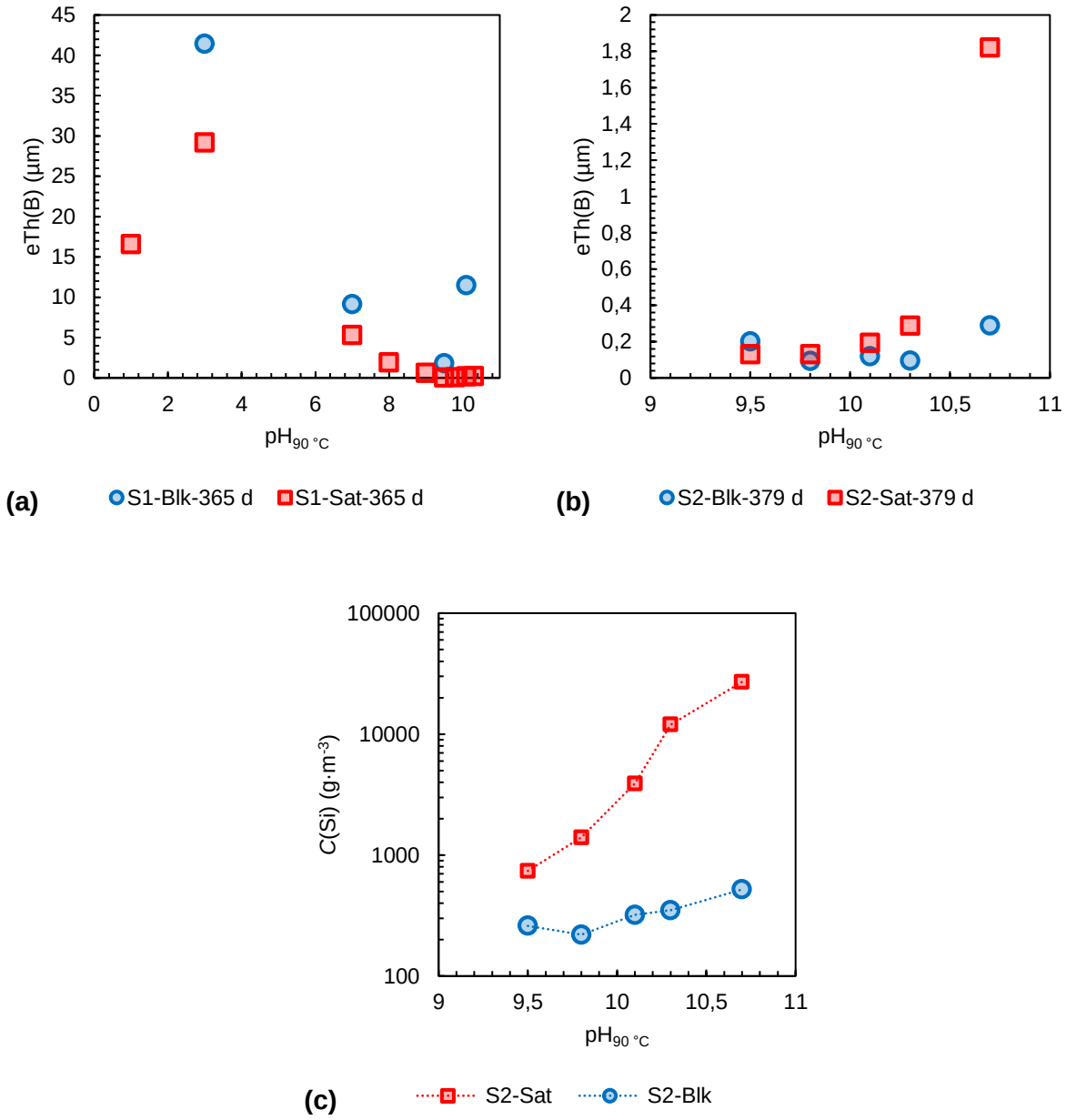

300 **Figure 6:** Comparison of the equivalent thicknesses of altered glass calculated from boron concentrations, eTh(B), at the last sampling time (≈ 1 year) for the various pH tested for **(a)** S1 test series and **(b)** S2 test series. **(c)** Comparison of the silicon concentrations, *C*(Si), reached at the end of the experiment (379 d) for the various pH tested for S2 test series.

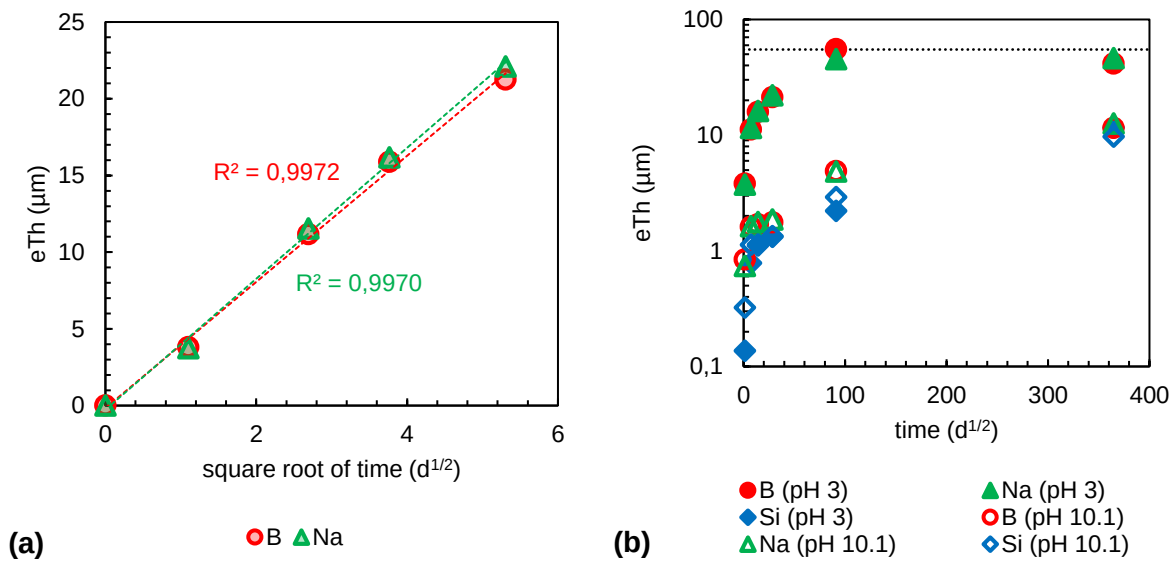

Figure 7: (a) Evolution of the equivalent thicknesses of altered glass, eTh, calculated from boron and sodium concentrations for the S1-Blk-3 test as the function of the square root of time during the first 14 days. **(b)** Comparison of the evolutions of B, Na, and Si eTh for the S1-Blk-3 (plain symbols) and S1-Blk-10.1 (open symbols) tests. Dotted line represents the total alteration of the glass (%AG = 100).

5. Conclusion

Test series show a negligible effect of aqueous silica at acidic pH and a marked effect beyond $pH_{90\,°C}$ = 7 at low reaction progress, ensuring a better glass chemical durability. Thus, pH-induced changes in solution chemistry shift equilibria. At higher reaction progress and for $pH_{90\,°C}$ ≥ 9.5, this effect becomes negative due to the formation of secondary phases (Figure 8). Most of the phases identified are hydroxides, which are likely precursors of better crystalized phases formed by Ostwald ripening.

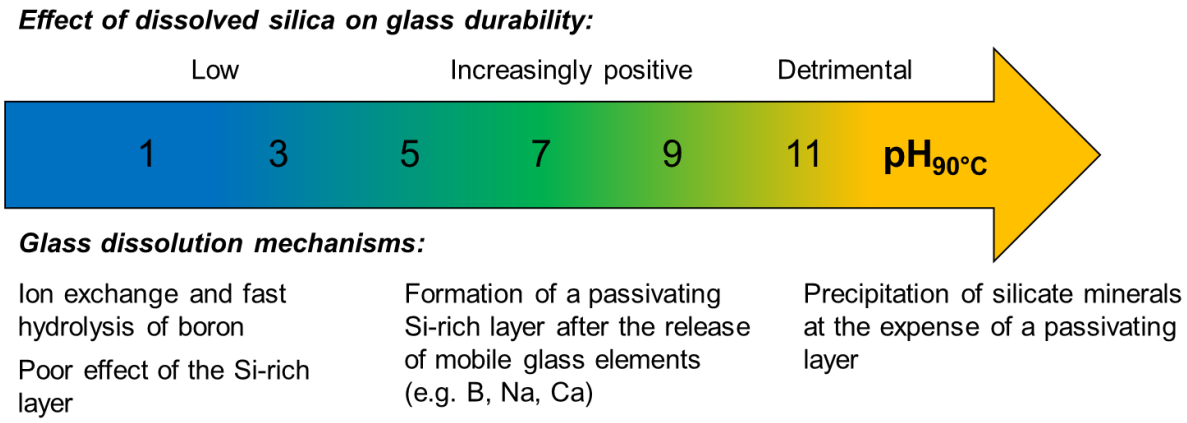

Figure 8: Diagram summarizing the effects of dissolved silica and glass dissolution mechanisms as a function of pH.

Acknowledgements

This research was supported by ANDRA. The authors are grateful to Jean-Pierre Mestre for SEM analysis, Géraldine Parisot and the laboratory CEA/DEN/DMRC/SA2I/LMAC for ICP-OES analysis.

References

[1] B. Grambow, Nuclear waste glasses; how durable?, Elements 2(6) (2006) 357-364.
[2] C. Fillet, I. Ribet, S. Gin, S. Peuget, E. Vernaz, Long term behaviour of French R7T7 glass: a short review, Glass Technology - European Journal of Glass Science and Technology Part A 49(6) (2008) 302-306.
[3] E. Curti, J.L. Crovisier, G. Morvan, A.M. Karpoff, Long-term corrosion of two nuclear waste reference glasses (MW and SON68): A kinetic and mineral alteration study, Appl. Geochem. 21(7) (2006) 1152-1168.
[4] B.M.J. Thien, N. Godon, A. Ballestero, S. Gin, A. Ayral, The dual effect of Mg on the long-term alteration rate of AVM nuclear waste glasses, J. Nucl. Mater. 427(1-3) (2012) 297-310.
[5] H. Arena, N. Godon, D. Rebiscoul, R. Podor, E. Garces, M. Cabie, J.P. Mestre, Impact of Zn, Mg, Ni and Co elements on glass alteration: Additive effects, Journal of Nuclear Materials 470 (2016) 55-67.
[6] H. Aréna, N. Godon, D. Rébiscoul, P. Frugier, R. Podor, E. Garcès, M. Cabie, J.P. Mestre, Impact of iron and magnesium on glass alteration: Characterization of the secondary phases and determination of their solubility constants, Appl. Geochem. 82 (2017) 119-133.
[7] M. Fournier, S. Gin, P. Frugier, S. Mercado-Depierre, Contribution of zeolite seeded experiments to the understanding of resumption of glass alteration, npj Mater. Degrad. 1 (2017) 17.
[8] E. Burger, D. Rebiscoul, F. Bruguier, M. Jublot, J.E. Lartigue, S. Gin, Impact of iron on nuclear glass alteration in geological repository conditions: A multiscale approach, Appl. Geochem. 31 (2013) 159-170.
[9] B. Fleury, N. Godon, A. Ayral, S. Gin, SON68 glass dissolution driven by magnesium silicate precipitation, J. Nucl. Mater. 442(1) (2013) 17-28.

[10] L. Neill, S. Gin, T. Ducasse, T. De Echave, M. Fournier, P. Jollivet, A. Gourgiotis, N.A. Wall, Various effects of magnetite on international simple glass (ISG) dissolution: implications for the long-term durability of nuclear glasses, npj Mater. Degrad. 1(1) (2017) 1.
[11] T. De Echave, M. Tribet, P. Jollivet, C. Marques, S. Gin, C. Jégou, Effect of clayey groundwater on the dissolution rate of SON68 simulated nuclear waste glass at 70 °C, J. Nucl. Mater. 503 (2018) 279-289.
[12] P. Frugier, S. Gin, Y. Minet, T. Chave, B. Bonin, N. Godon, J.E. Lartigue, P. Jollivet, A. Ayral, L. De Windt, G. Santarini, SON68 nuclear glass dissolution kinetics: Current state of knowledge and basis of the new GRAAL model, J. Nucl. Mater. 380(1-3) (2008) 8-21.
[13] P. Frugier, Y. Minet, N. Rajmohan, N. Godon, S. Gin, GRAAL, a model for glass corrosion, npj Mater. Degrad. submitted (2018).
[14] P. Van Iseghem, M. Aertsens, S. Gin, D. Deneele, B. Grambow, D. Strachan, P. McGrail, G. Wicks, GLAMOR - Or how we achieved a common understanding on the decrease of glass dissolution kinetics, Ceram. Trans. 207(s) (2009) 115-126.
[15] J.P. Icenhower, B.P. McGrail, W.J. Shaw, E.M. Pierce, P. Nachimuthu, D.K. Shuh, E.A. Rodriguez, J.L. Steele, Experimentally determined dissolution kinetics of Na-rich borosilicate glass at far from equilibrium conditions: Implications for Transition State Theory, Geochim. Cosmochim. Acta 72(12) (2008) 2767-2788.
[16] J. Neeway, A. Abdelouas, B. Grambow, S. Schumacher, Dissolution mechanism of the SON68 reference nuclear waste glass: New data in dynamic system in silica saturation conditions, J. Nucl. Mater. 415(1) (2011) 31-37.
[17] S. Gin, P. Frugier, P. Jollivet, F. Bruguier, E. Curti, New insight into the residual rate of borosilicate glasses: Effect of S/V and glass composition, Int. J. Appl. Glass Sci. 4(4) (2013) 371-382.
[18] S. Gin, P. Frugier, SON68 glass dissolution kinetics at high reaction progress: Experimental evidence of the residual rate, Mater. Res. Soc. Symp. Proc. 757 (2003) II5.9.
[19] T. Advocat, J.L. Chouchan, J.L. Crovisier, C. Guy, V. Daux, C. Jegou, S. Gin, E. Vernaz, Borosilicate nuclear waste glass alteration kinetics: Chemical inhibition and affinity control, Mater. Res. Soc. Symp. Proc. 506 (1998) 63-70.
[20] P. Jollivet, S. Gin, S. Schumacher, Forward dissolution rate of silicate glasses of nuclear interest in clay-equilibrated groundwater, Chem. Geol. 330-331 (2012) 207-217.
[21] S. Mercado-Depierre, F. Angeli, F. Frizon, S. Gin, Antagonist effects of calcium on borosilicate glass alteration, J. Nucl. Mater. 441(1) (2013) 402-410.
[22] T. Chave, P. Frugier, S. Gin, A. Ayral, Glass-water interphase reactivity with calcium rich solutions, Geochim. Cosmochim. Acta 75(15) (2011) 4125-4139.
[23] P. Jollivet, P. Frugier, G. Parisot, J.P. Mestre, E. Brackx, S. Gin, S. Schumacher, Effect of clayey groundwater on the dissolution rate of the simulated nuclear waste glass SON68, J. Nucl. Mater. 420(1-3) (2012) 508-518.
[24] H. Aréna, D. Rébiscoul, R. Podor, E. Garcès, M. Cabie, J.P. Mestre, N. Godon, Impact of Fe, Mg and Ca elements on glass alteration: Interconnected processes, Geochim. Cosmochim. Acta 239 (2018) 420-445.
[25] B. Craeye, G. De Schutter, H. Van Humbeeck, A. Van Cotthem, Concrete containers for containment of vitrified high-level radioactive waste: The Belgian approach, CRC Press-Taylor & Francis Group, Boca Raton, 2009.
[26] S. Gin, A. Abdelouas, L.J. Criscenti, W.L. Ebert, K. Ferrand, T. Geisler, M.T. Harrison, Y. Inagaki, S. Mitsui, K.T. Mueller, J.C. Marra, C.G. Pantano, E.M. Pierce, J.V. Ryan, J.M. Schofield, C.I. Steefel, J.D. Vienna, An international initiative on long-term behavior of high-level nuclear waste glass, Mater. Today 16(6) (2013) 243-248.
[27] S. Gin, P. Jollivet, M. Fournier, C. Berthon, Z. Wang, A. Mitroshkov, Z. Zhu, J.V. Ryan, The fate of silicon during glass corrosion under alkaline conditions: A mechanistic and kinetic study with the International Simple Glass, Geochim. Cosmochim. Acta 151 (2015) 68-85.
[28] M. Fournier, A. Ull, E. Nicoleau, Y. Inagaki, M. Odorico, P. Frugier, S. Gin, Glass dissolution rate measurement and calculation revisited, J. Nucl. Mater. 476 (2016) 140-154.
[29] J. van der Lee, L. De Windt, V. Lagneau, P. Goblet, Module-oriented modeling of reactive transport with HYTEC, Comput. Geosci. 29(3) (2003) 265-275.

[30] ASTM International, Standard test method for silica in water, ASTM Standard S859, West Conshohocken, PA, United-States, 2010.
[31] S. Depierre, Etude des mécanismes d'altération du verre par des eaux cimentaires, Thèse de l'Université Montpellier 2, 2012.
[32] B. Thien, N. Godon, F. Hubert, F. Angéli, S. Gin, A. Ayral, Structural identification of a trioctahedral smectite formed by the aqueous alteration of a nuclear glass, Appl. Clay Sci. 49(3) (2010) 135-141.
[33] C. Zhu, D.R. Veblen, A.E. Blum, S.J. Chipera, Naturally weathered feldspar surfaces in the Navajo Sandstone aquifer, Black Mesa, Arizona: Electron microscopic characterization, Geochim. Cosmochim. Acta 70(18) (2006) 4600-4616.
[34] J.R. Houston, R.S. Maxwell, S.A. Carroll, Transformation of meta-stable calcium silicate hydrates to tobermorite: reaction kinetics and molecular structure from XRD and NMR spectroscopy, Geochem. Trans. 10 (2009).
[35] J.M. Fernández, A. Duran, I. Navarro-Blasco, J. Lanas, R. Sirera, J.I. Alvarez, Influence of nanosilica and a polycarboxylate ether superplasticizer on the performance of lime mortars, Cem. Concr. Res. 43 (2013) 12-24.
[36] Y. Inagaki, T. Kikunaga, K. Idemitsu, T. Arima, Initial dissolution rate of the International Simple Glass as a function of pH and temperature measured using microchannel flow-through test method, Int. J. Appl. Glass Sci. 4(4) (2013) 317-327.
[37] S. Gin, P. Jollivet, M. Fournier, F. Angeli, P. Frugier, T. Charpentier, Origin and consequences of silicate glass passivation by surface layers, Nat. Commun. 6 (2015) 6360.
[38] S. Mitsui, R. Aoki, Effect of a siliceous additive on aqueous alteration of waste glass with engineered barrier materials, J. Nucl. Mater. 298(1-2) (2001) 184-191.
[39] K. Ferrand, A. Abdelouas, B. Grambow, Water diffusion in the simulated French nuclear waste SON 68 contacting silica rich solutions: Experimental and modeling, J. Nucl. Mater. 355 (2006) 54-67.
[40] M.I. Ojovan, A. Pankov, W.E. Lee, The ion exchange phase in corrosion of nuclear waste glasses, J. Nucl. Mater. 358(1) (2006) 57-68.
[41] B.C. Bunker, Molecular mechanisms for corrosion of silica and silicate glasses, J. Non-Cryst. Solids 179 (1994) 300-308.
[42] R.K. Iler, The Chemistry of Silica: Solubility, Polymerization, Colloid and Surface Properties, and Biochemistry of Silica, John Wiley & Sons Inc.1979.
[43] D. Daval, S. Bernard, L. Rémusat, B. Wild, F. Guyot, J.S. Micha, F. Rieutord, V. Magnin, A. Fernandez-Martinez, Dynamics of altered surface layer formation on dissolving silicates, Geochim. Cosmochim. Acta 209 (2017) 51-69.
[44] D. Daval, I. Martinez, J.-M. Guigner, R. Hellmann, J.r.m. Corvisier, N. Findling, C. Dominici, B. Goffé, F.o. Guyot, Mechanism of wollastonite carbonation deduced from micro- to nanometer length scale observations, Am. Mineral. 94(11-12) (2009) 1707-1726.
[45] G. Jordan, S.R. Higgins, C.M. Eggleston, S.M. Swapp, D.E. Janney, K.G. Knauss, Acidic dissolution of plagioclase: in-situ observations by hydrothermal atomic force microscopy, Geochim. Cosmochim. Acta 63(19) (1999) 3183-3191.
[46] R. Hellmann, J.M. Penisson, R.L. Hervig, J.H. Thomassin, M.F. Abrioux, An EFTEM/HRTEM high-resolution study of the near surface of labradorite feldspar altered at acid pH: evidence for interfacial dissolution-reprecipitation, Phys. Chem. Miner. 30(4) (2003) 192-197.
[47] B. Wild, D. Daval, F. Guyot, K.G. Knauss, M. Pollet-Villard, G. Imfeld, pH-dependent control of feldspar dissolution rate by altered surface layers, Chem. Geol. 442 (2016) 148-159.
[48] G.D. Saldi, D. Daval, G. Morvan, K.G. Knauss, The role of Fe and redox conditions in olivine carbonation rates: An experimental study of the rate limiting reactions at 90 and 150°C in open and closed systems, Geochim. Cosmochim. Acta 118 (2013) 157-183.
[49] M. Fournier, S. Gin, P. Frugier, Resumption of nuclear glass alteration: State of the art, J. Nucl. Mater. 448(1-3) (2014) 348-363.
[50] S. Gin, X. Beaudoux, F. Angéli, C. Jégou, N. Godon, Effect of composition on the short-term and long-term dissolution rates of ten borosilicate glasses of increasing complexity from 3 to 30 oxides, J. Non-Cryst. Solids 358(18-19) (2012) 2559-2570.

[51] S. Mercado-Depierre, M. Fournier, S. Gin, F. Angeli, Influence of zeolite precipitation on borosilicate glass alteration under hyperalkaline conditions, J. Nucl. Mater. 491 (2017) 67-82.
[52] W.L. Bourcier, D.W. Peiffer, K.G. Knauss, K.D. McKeegan, D.K. Smith, A kinetic model for borosilicate glass dissolution affinity of a surface alteration layer., Mater. Res. Soc. Symp. Proc. 176 (1989) 209-216.
[53] I. Munier, J.L. Crovisier, Alteration of Si-B-Na-Al model glass in water at 90 °C: experiments and thermodynamic modelling, Mater. Res. Soc. Symp. Proc. 757 (2003) 153-158.

Appendix A

In the tests conducted in this study, the pH was manually regulated around a set value. Figures A.1 (for S1 test series) and A.2 (for S.2 test series) show the different setpoint pH (dashed lines), the measured pH (circles) and the pH reached after addition of micro-volumes of KOH or HNO_3 solutions if necessary (crosses).

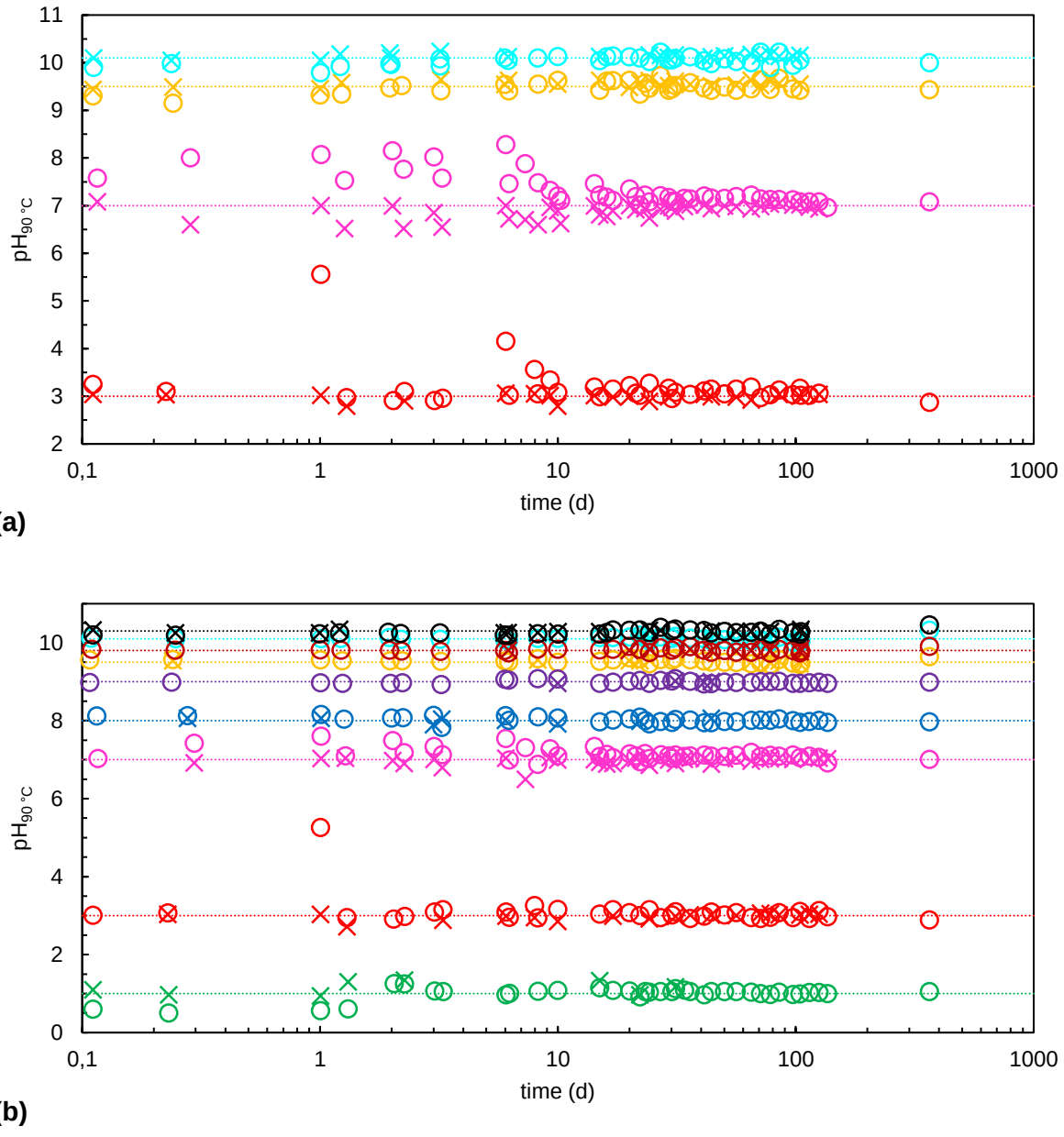

Figure A.1: pH measured in S1 test series **(a)** "Blk" and **(b)** "Sat" before regulation (○) and after regulation (×) around set values (dotted lines) at $pH_{90\,°C}$ = 1 (green), 3 (red), 7 (pink), 8 (blue), 9 (purple), 9.5 (orange), 9.8 (dark red), 10.1 (light blue), and 10.3 (black).

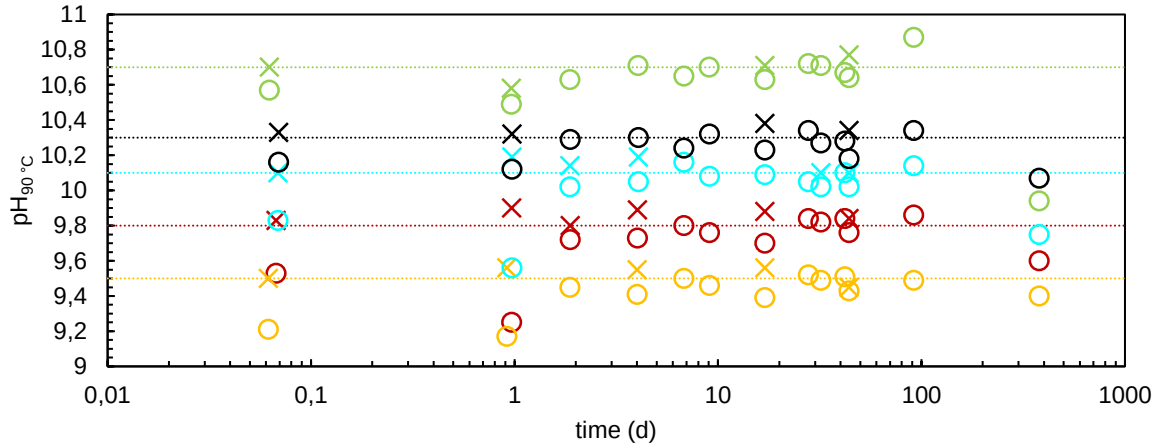

(a)

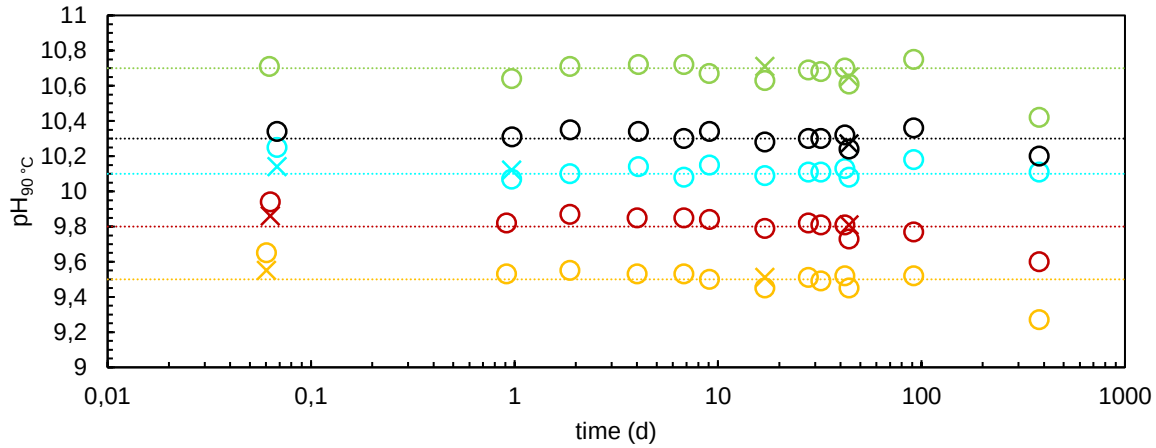

475 **(b)**

Figure A.2: pH measured in S2 test series **(a)** "Blk" and **(b)** "Sat" before regulation (○) and after regulation (×) around set values (dotted lines) at $pH_{90\,°C}$ = 9.5 (orange), 9.8 (dark red), 10.1 (light blue), and 10.3 (black), and 10.7 (light green).

Appendix B

Zoomed-in subfigures of Figure 1 and Figure 3 are given in Figure B.1 and Figure B.2, respectively.

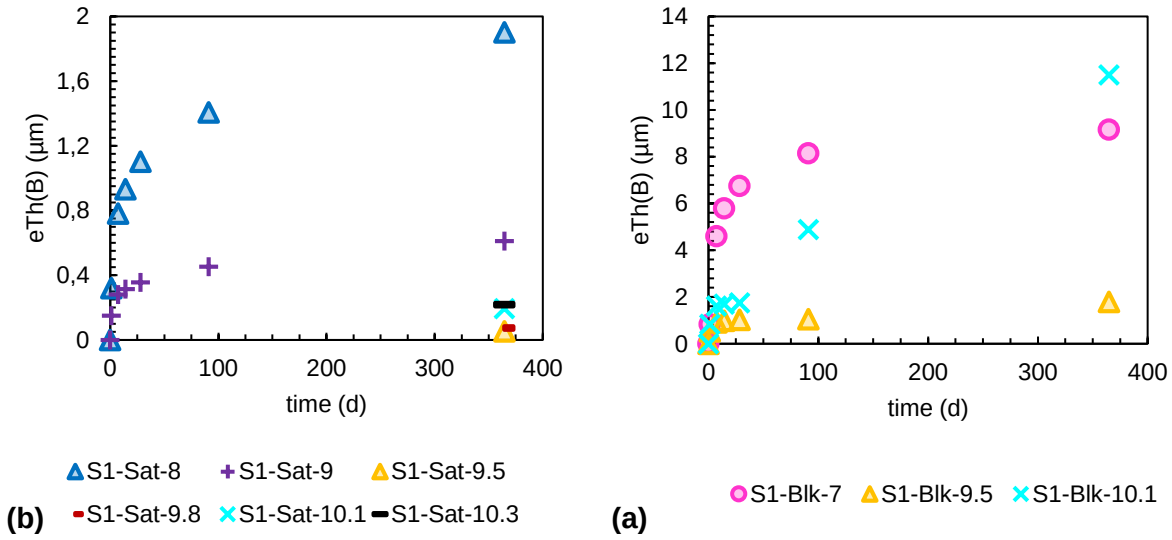

Figure B.1: Zoomed-in subfigures of **(a)** Figure 1.a and **(b)** Figure 1.b.

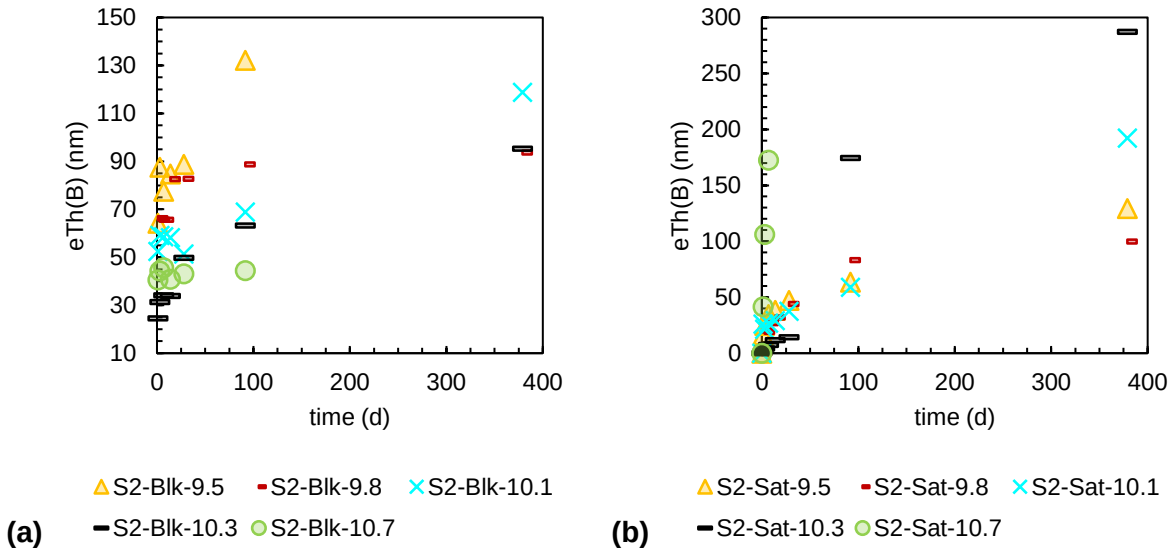

Figure B.1: Zoomed-in subfigures of **(a)** Figure 3.a and **(b)** Figure 3.b.

Appendix C

A direct comparison between the “Blk” and “Sat” tests for the two test series of tests at all sampling dates is shown in Figures C.1 and C.2.

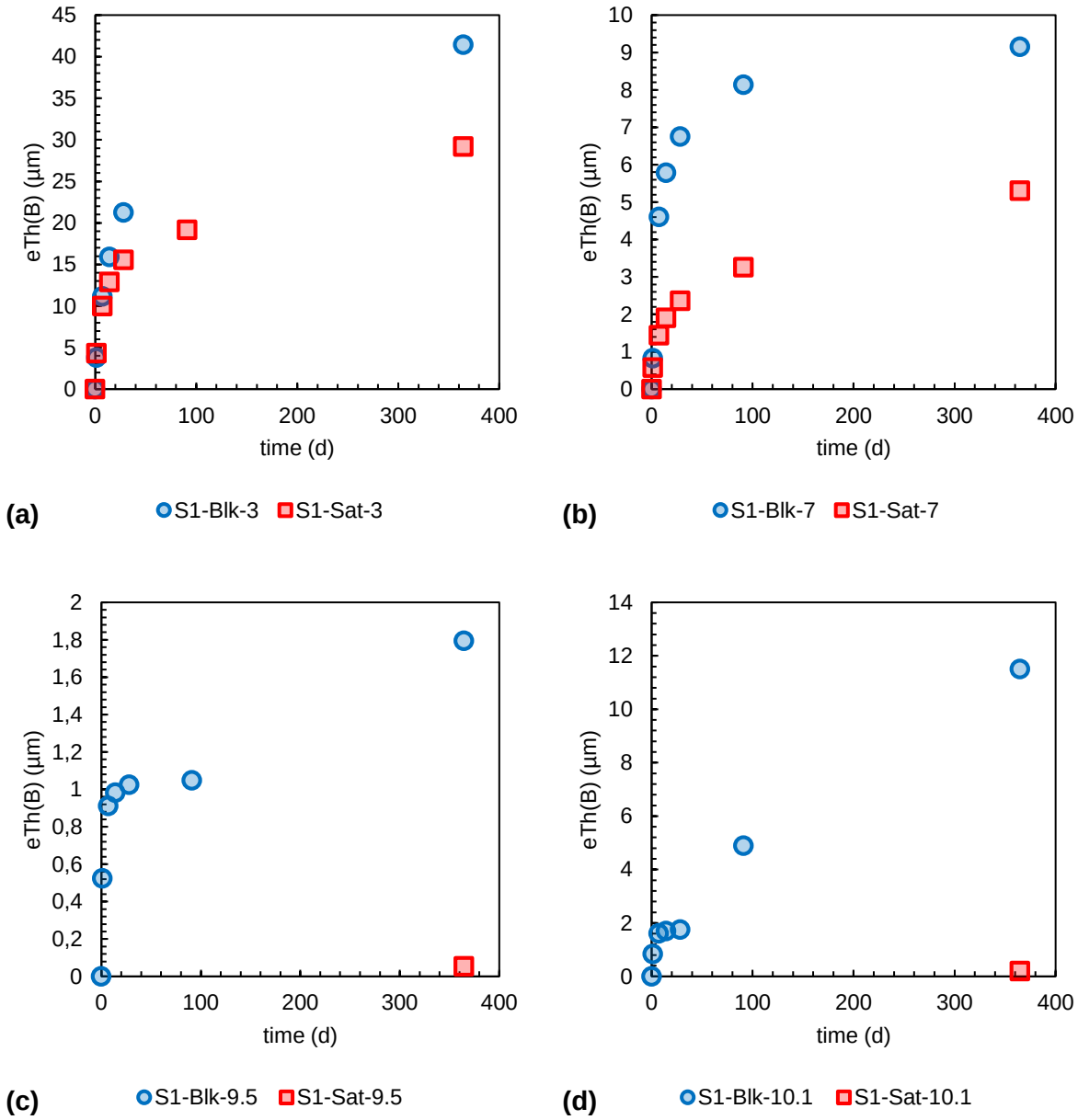

Figure C.1: Comparative evolution of the equivalent thicknesses of altered glass calculated from boron concentrations, eTh(B), for S1 test series conducted with a *S*/*V* ratio of 60 m^{-1} at $pH_{90\,°C}$ equal to **(a)** 3, **(b)** 7, **(c)** 9.5, and **(d)** 10.1.

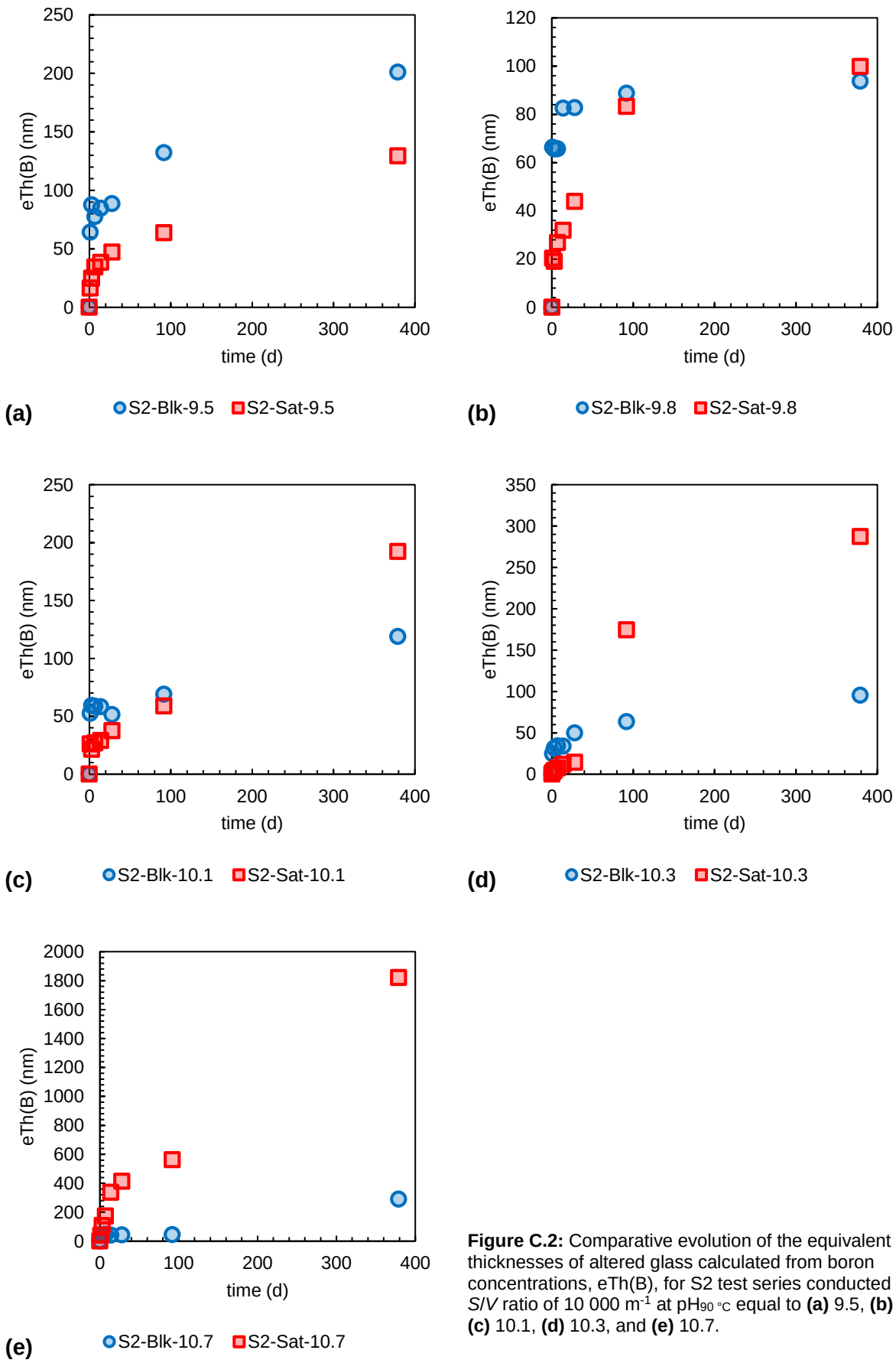

Figure C.2: Comparative evolution of the equivalent thicknesses of altered glass calculated from boron concentrations, eTh(B), for S2 test series conducted with a *S*/*V* ratio of 10 000 m^{-1} at $pH_{90\ °C}$ equal to **(a)** 9.5, **(b)** 9.8, **(c)** 10.1, **(d)** 10.3, and **(e)** 10.7.